AN INVESTIGATION OF THE DYNAMIC BEHAVIOUR OF ASYMMETRIC SPINNAKERS AT FULL-SCALE

Dario Motta[1], dmot267@aucklanduni.ac.nz
Richard Flay[1], r.flay@auckland.ac.nz
Peter Richards[1], pj.richards@auckland.ac.nz
David Le Pelley[1], d.lepelley@auckland.ac.nz
Patrick Bot[2], patrick.bot@ecole-navale.fr
Julien Deparday[2], julien.deparday@ecole-navale.fr

Abstract. This paper presents new results obtained from analysing on-the-water pressure, shape, force, speed and direction data that were obtained from experiments in the Hauraki Gulf in Auckland, New Zealand in April 2014. A fully instrumented Stewart 34 Class yacht sailing downwind was used for the tests. Details of the analysis of the results from simultaneous time-resolved measurements of pressure, sail shape and loads are presented. The dynamic behaviour of the fluid-structure system made up of a light sail cloth and highly curved flow is investigated. Aerodynamic forces on the asymmetric spinnaker are determined from the combination of point pressure measurements across the sail with simultaneous shape measurements. Simultaneous time histories show a strong correlation between the variations of pressure distributions, flapping sail shape and the forces at the corners. Periodic curling and filling of the spinnaker luff influences suctions, in particular at the leading edge, and forces, which can dynamically change on the order of 40-50%. The results are similar to, and extend, those that were presented by the authors at the 2013 Innov'sail Conference in Lorient, France. It is expected that the results from this work will give reliable benchmark data which may be used to validate unsteady fluid-structure interaction numerical simulations of downwind sails.

NOMENCLATURE

A	Total sail area (m²)
A_{main}	Main sail area (m²)
A_{spi}	Spinnaker or gennaker area (m²)
AWA	Apparent wind angle (°)
AWS	Apparent Wind Speed (m/s)
CF_{TOT}	Total Aerodynamic Force Coefficient
CF_X	Total Driving Force Coefficient
CF_{Xmain}	Driving Force Coefficient for the main sail only
CF_{Xspi}	Driving Force Coefficient for the spinnaker only
CMh	Total Heeling Moment Coefficient
CMh_{main}	Heeling Moment Coefficient for the main sail only
CMh_{spi}	Heeling Moment Coefficient for the spinnaker only
ΔC_P	Differential pressure Coefficient
$FEPV$	Force Evaluation via Pressures and VSPARS
Fx	Total Driving Force (N)
Mh	Total Heeling Moment (N.m)
TWS	True Wind Speed (m/s)
VSPARS	Visual Sail Position and Rig Shape
Vs	Boat Speed (m/s)

1. INTRODUCTION

Wind tunnel testing [1-2] and numerical simulations [3-4] are widely used to improve the understanding of downwind sail aerodynamics. Recently, numerical models [5] in particular have provided fresh insights into fluid-structure interactions. However, both methods have various drawbacks [6]. Full-scale testing is usually required to validate results from these methods, since this allows the investigation of sail aerodynamics in real sailing conditions.

On-water experiments can focus on different aspects of sail aerodynamics and yacht design in general. Determination of the pressure distributions on the sails [7-9], measuring loads on the rigging [10], investigation the influence of rigging on yacht performance [11], determining the total aerodynamic forces and loads by means of sailing dynamometers [12-13], are all possible applications of full-scale testing.

At the Yacht Research Unit of the University of Auckland significant efforts are being made to develop a method for investigating sail aerodynamics at full scale. This method, which has been given the name FEPV (Force Evaluation via Pressures and VSPARS) combines simultaneous on-water pressure and sail shape measurements to obtain the aerodynamic forces and moments produced by sails at full scale, where the VSPARS system is used to ascertain the sail shape. Le Pelley et al. [7] presented the results of the first full-scale test carried out using the FEPV system and a validation of the full system through wind tunnel testing for upwind sailing. Bergsma et al. [11] describe an application of the FEPV system to upwind sailing, where the effects of shroud tension on upwind sailing performance were investigated. Motta et al. [8] extended the application of FEPV from upwind to downwind sailing, presenting the results from downwind full-scale tests on a Stewart 34 Class yacht in very light winds in New Zealand, and on a J80 Class yacht in stronger winds in France. In all the mentioned works, sail aerodynamics were studied by analysing time-averaged values of pressures, sail shape

1 Yacht Research Unit, Department of Mechanical Engineering, University of Auckland, New Zealand
2 Naval Academy Research Institute, France

and forces. Averaging the results over 20 seconds allowed the calculation of characteristic values of the parameters of interest for given wind direction and speed. A step forward in the development of the FEPV method and the full-scale technique in general has been the investigation of the dynamic behaviour of asymmetric spinnakers in real sailing conditions [14].

The present paper illustrates new results obtained from experiments on the Hauraki Gulf in Auckland, New Zealand in April 2014. A fully instrumented Stewart 34 Class yacht sailing downwind was used for the tests. Details of the analysis of the results from simultaneous time-resolved measurements of pressure, sail shape and loads are presented.

In the current work, in order to better assess the aerodynamic forces, a higher number of taps, compared to Deparday et al. [14], were placed on the sail (72 instead of 42), as described in section 3. In addition, pressure transducers were placed at the foot and very close to the head of the sails.

2. COMPONENTS OF FEPV SYSTEM

2.1 VSPARS and sail shape measurements

VSPARS is a system that can be used to capture the sail shape both in the wind tunnel and at full scale. It was developed in the Yacht Research Unit (YRU) at the University of Auckland by Le Pelley and Modral [15]. It uses cameras mounted at deck level looking upwards at the sails and rig. The system determines the global locations in Cartesian coordinates of specific targets on the sails and rig. For the rig, these targets comprise coloured dots which are placed at different heights on the mast, typically under the spreaders or at diagonal crosses. On the sails, coloured horizontal stripes are applied to the mainsail, jib and downwind sails. The system is able to dynamically track the stripes, calculate the stripe coordinates in 3D space, and link the stripe positions to the rig deflection.

The main advantage of VSPARS over other systems is that it is able to deal with large perspective effects. Even systems that look up or down at the stripes from the centre of the chord can still have significant perspective effects at the luff and leech ends of the stripes. By accounting for these effects, it is possible to place a camera in the optimum position to see as much of the sail as possible whilst still producing an accurate sail shape, as is done in the VSPARS system. This also enables the system to cope with large changes in sheeting angle. It has been shown to work well even for the highly curved stripes in off-wind sails [15]. The main steps of the software can be seen in Figure 1. The program essentially takes images using the required camera(s), automatically finds the sail stripes and rig targets, and then combines the results of all the data to give the global X, Y and Z coordinates of the sail stripes and rig relative to the boat fixed origin of the coordinate system.

Further details on VSPARS performance can be found in [15].

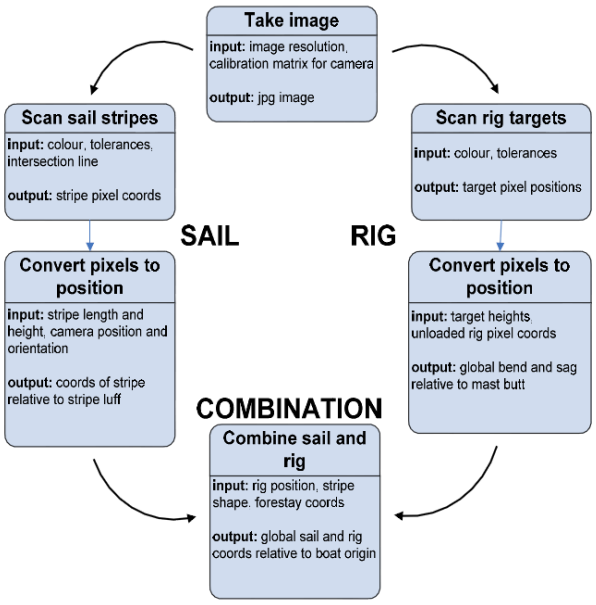

Figure 1: VSPARS system flow chart

2.2 Pressure measurement system

The pressure measurement system was custom-built by the Yacht Research Unit at the University of Auckland. The generic layout of the system, as applied to each sail, is shown in Figure 2a. Ultra-low range differential pressure sensors (Honeywell XSCL04DC) are the core of the system. The sensors' resolution and range fit the criteria for sailing applications. The pressure sensors are mounted in custom plastic housings, approximately 40 mm in diameter and 10 mm thick. On one side, they are stuck to the sail, with a small hole melted through the sail to a pressure port on the bottom surface of the housing. On the other side, a light sail cloth patch, approximately 150 mm x 150 mm in area, is applied with another hole through to the opposite pressure port, as shown in Figure 2b. The differential pressure between the two sides is measured. Using this setup, transducers are placed directly at the measuring locations, thus avoiding the issues associated with the use of long tubing and the recording of a reliable static reference pressure [16].

An operational amplifier (op-amp) is connected directly onto each transducer which amplifies its analogue output from a few mV to a signal in the ±2.5 V range. Using IDC (Insulation Displacement Contact) connectors the transducers are connected to a ribbon cable running along the chord of the sail. Each chord-wise cable terminates on an analogue-to-digital (ADC) converter chip which converts the analogue voltage signal into a

12-bit digital signal. A maximum of 8 taps can be connected to each ADC. For upwind sails this seems to be a sufficient number of taps to catch an accurate chord-wise pressure distribution. For downwind sails it is necessary to increase the number of taps per row because of the more highly varying pressure distributions, and thus two separate systems have been mounted "in parallel" on the sail in the present measurements.

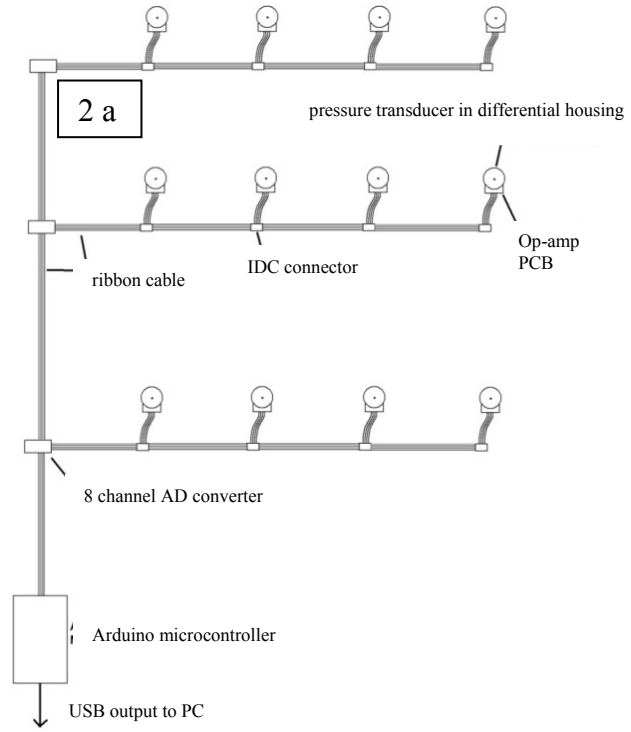

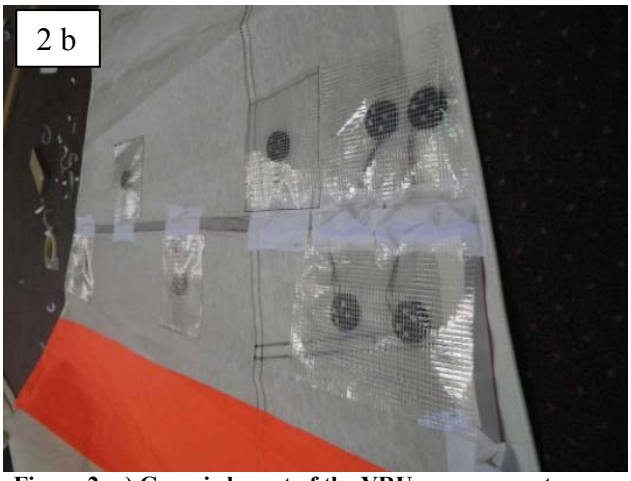

Figure 2: a) Generic layout of the YRU pressure system as applied to a sail; b) Example of application of pressure sensors on the sail showing the pockets containing the sensors

The current system handles 9 ADCs and therefore 9 sets of 8 transducers. The ADC chips are connected to a continuous ribbon cable along the luff of the sail which terminates at a USB-driven microcontroller box placed at the tack. The microcontroller combines the data from all of the taps on the sail and sends them in a single sentence back to the data acquisition PC. The system can sample over 150 sensors at a rate of 20 Hz, which is higher than required for sailing applications where 4-5 Hz is probably sufficient. If necessary, in order to reduce the effect of electrical noise, the signal can be averaged over a number of readings from each transducer, resulting in a lower effective frequency.

2.3 FEPV Data Analysis

The FEPV analysis was coded in Matlab, and uses the output files from VSPARS and the pressure system to obtain the aerodynamic forces and moments. The whole sail surface is created from the recorded stripe shapes and the known tack and head positions from physical measurements *a priori*. The head is assumed to be flat (with no camber) and to have a small finite length. A spline curve, joining the leech points of the recorded stripes, is extrapolated upwards to the known head height position and also downwards using the known leech length of the sail, to give the head and foot twists respectively, together with the first estimate of the clew position. Unfortunately the foot shape cannot be captured by the camera as it is out of the viewing area with the present VSPARS setup. Therefore an initial foot shape is estimated by fitting a spline curve through the known tack and clew positions together with a 3rd point given by an estimated foot depth and draft position, obtained by extrapolating the depth and draft position of the known stripes. This foot shape is then scaled in both the longitudinal and transverse directions to match the known foot length. Starting from the "low resolution" sail shape defined by the VSPARS stripes and the foot and head positions, a fine quadrilateral mesh is then interpolated over the sail surface.

The sail pressure distributions are obtained from the discrete pressure values recorded by the pressure system by interpolation. The interpolation scheme is based on the Radial Basis Function of order 1 (linear), which is a real-valued function whose value depends only on the distance from the reference points, called centres (the pressure taps in this application). Pressure tap positions are defined intrinsically to the sail shape in terms of chord-wise and span-wise percentages. Moreover the use of this interpolation scheme allows a scattered set of pressure measurements to be extrapolated over the sail. The pressures are interpolated to the centre of each geometrical cell in order to obtain a pressure map distribution over the entire surface of both sails. Forces in specified directions are computed by integrating the known pressures acting over the cell areas taking into account their surface normal directions. Moment contributions from each cell are calculated about the specified yacht moment reference centre. In the present case the moment reference centre was fixed at the base of the mast.

3. FULL SCALE TEST SETUP

A Stewart 34 class yacht was used for the full-scale testing in New Zealand. Class rules impose the use of a symmetric spinnaker, but for these tests the yacht has been equipped with an asymmetric spinnaker designed by North Sails New Zealand.

A GPS unit, sampling at a rate of 2.5 Hz, was used to record the speed over ground, course over ground and boat location. An Inertial Measurement Unit (IMU) was placed in the yacht cabin and logged the boat motion at 10 Hz. A sonic anemometer placed 1.2 m above the masthead recorded the wind speed and direction in 3 dimensions. In addition two GoPro cameras, placed at the stern and looking forwards, recorded the crew activity and trimming of the spinnaker.

The asymmetric spinnaker was equipped with the YRU pressure measurement system (described in Section 2.2). Pressures were recorded at approximately 10 Hz. Taps were placed at six different chord-wise stripes along the sail, which are named: foot, S1/5, S2/5, S3/5, S4/5 and S15/16 respectively. The name S1/5 indicates that the stripe starts on the luff at 20% (i.e. 1/5) of the luff length from the foot and ends on the leech, at 20% of the leech length from the clew; sensors are placed on the curve joining these two points. Tap locations as a percentage of the curve length from the luff are shown in Table 1. Based on previous experience [8], the authors decided to use the maximum number of pressure taps available, namely 72. Some taps were placed as close as possible to the sail foot and close to the sail head, since these have never been measured at full-scale to best of the authors' knowledge.

The VSPARS system recorded the sail shape for the spinnaker by means of two GoPro cameras (one camera for each tack), used in video mode. Images were then extracted from the video at 10 frames per second.

The spinnaker was equipped with four VSPARS orange stripes, placed at 1/4, 1/2, 3/4 and 7/8 of the luff length from the tack respectively. The stripes were laid on the sail in order to fly approximately horizontally (in the yacht's reference system) whilst sailing. A further orange stripe was placed at height 1/8 but, as the authors expected, it fell outside the camera's field of view and so was not used during the data post-processing. The general specifications of the spinnaker and VSPARS stripe lengths are shown in Table 2.

A custom-made data acquisition unit recorded all data streams, each one at its own sampling rate, and so the data were all time stamped to enable subsequent synchronous processing. During the post-processing, all measurements were resampled at 10 Hz and smoothed with an exponential moving average in order to remove some unexpected peaks.

Table 1: Taps locations expressed as percentage of the curve length

	Foot	S 1/5	S 2/5	S 3/5	S 4/5	S 15/16
length / tap no	7780 mm	8684 mm	8614 mm	7140 mm	4040 mm	1730 mm
1	7	0.6	0.6	0.7	1.2	10
2	10	3	3	3.0	3	35
3	15	5	5	5.0	5	65
4	25	7.5	7.5	7.5	10	90
5	40	10	10	10	15	
6	60	15	15	15	25	
7	80	20	20	20	35	
8	94	25	25	25	45	
9		30	30	30	60	
10		35	35	35	75	
11		50	50	50	90	
12		60	60	60	99	
13		70	70	70		
14		80	80	80		
15		90	90	90		
16		99.4	99.4	99.4		

Table 2: Stewart 34 asymmetric spinnaker characteristics

Spinnaker area	88.6	m^2
Luff length	13000	mm
Leech length	12260	mm
Mast height	12800	mm
VSPARS stripe 7/8 length	2740	mm
VSPARS stripe 3/4 length	5142	mm
VSPARS stripe 1/2 length	8022	mm
VSPARS stripe 1/4 length	8628	mm

The measurements were performed in the Hauraki Gulf, Auckland, NZ, with a breeze of 10-15 knots, in an area with insignificant tidal flow with almost flat water.

4. RESULTS

Investigating the dynamic behaviour of an asymmetric spinnaker at full scale is not an easy task. The wind is constantly changing, the yacht is moving and the spinnaker itself has very large displacements that influence pressures and forces. In order to understand pressure and force variation it is important to identify time windows in which as many parameters as possible are constant, so that the changes can be related to the remaining fluctuating variables.

In section 4.1 pressure averages over 20s are shown in order to give an overview of the spinnaker behaviour. In section 4.2 and 4.3 two different cases are shown and discussed in order to explain the dynamic behaviour of the spinnaker. In section 4.2, the spinnaker was slightly overtrimmed and the sail was quite stable (no curling occurring near the luff), while in section 4.3 the spinnaker was on the verge of luffing, as is common practice among sailors.

4.1 Overview of time averaged pressures

Sailing downwind is unsteady by nature, due to the wind conditions, waves, helming and the sails' movement. To determine averaged forces and pressure distributions at different AWAs, time periods of about 20 seconds were chosen where the standard deviation of the AWA was below 5° and of the AWS below 0.5 m/s. Sail trim (optimal sail trim with gennaker on the verge of luffing) was kept constant for each run and the boat heading was kept as straight as possible to enable the results to be averaged.

Figures 3 shows an example of averaged differential pressure coefficient (ΔC_P) distributions for all the pressure stripes on the spinnaker for AWA equal to 98°. ΔC_P is plotted against the sail curve length percentage. The dynamic pressure was calculated from the apparent wind speed (AWS), and the pressure differences are leeward minus windward, thus giving negative values.

The pressure coefficient plots have the negative direction upwards, as is common in presenting pressure distributions on wings. The standard deviation for ΔC_P at stripe 3/5 is shown as well for reference.

Figure 3 shows that suctions generally increase from the foot upwards to section 4/5 and then reduce to the head. For the lower stripes (1/5 and 2/5) there is a suction peak at about 5-7% from the leading edge followed by a recovery down to the trailing edge. A plateau in the pressure distribution or a second suction peak can sometimes be seen at about 20-30% of the curve, such as with section 1/5.

At stripes 3/5 and 4/5 the flow is probably separated, as indicated by the weak pressure recovery after the leading edge pressure peak. This difference in behaviour between the higher and lower sections confirms what has been already seen in earlier studies of asymmetric spinnakers on both the Stewart 34 and J80 yachts [8].

Even in stable wind conditions (standard deviation of AWA and AWS less than 5 deg and 0.5 m/s respectively) pressure variations along the curve are big, particularly near the leading edge and at higher stripes. Standard deviation of ΔC_P in the proximity of the leading edge is equal to approximately 1.7 at S3/5 and S4/5 and 1.2 at S1/5.

One novel aspect of the present study is information on the pressures at the foot and very close to the head (namely at 880 mm from the head). Time-averaged differential pressure coefficients at the foot as high as -3.5 are obtained. It appears that these differential pressure increase from near zero at the tack, reach a maximum about a quarter of the way along the foot and then decrease again. Also the ΔC_P variations along the foot are not negligible, having a maximum standard deviation of about 1.04 at 15% from the luff. The first pressure tap at the foot is placed at some distance (7%) from the luff and therefore a suction peak, if present, was not measured, either because too small or too close to the leading edge. This trend is repeated for all the range of AWAs investigated.

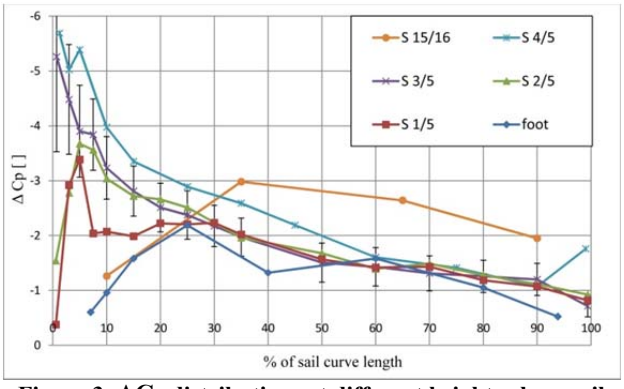

Figure 3: ΔC_P distributions at different heights along sail for AWA = 98°.

As mentioned in Section 3, a line of 4 pressure taps was placed at 15/16th of the sail height, thus very close to the sail head. Other than giving some new interesting information on the pressures in such locations, knowledge of these pressures was very beneficial in improving the interpolation of pressure over the whole sail in the FEPV code. Unfortunately, limitations on the number of taps meant that only 4 taps were placed closed to the head. As expected in this case, the suctions are not close to zero, but have significant values at all AWAs. In the example shown in Figure 3, maximum suction is achieved at about 35% of the curve and has a ΔC_P value of -3, while standard deviations are approximately equal to 0.4-0.6 over the whole stripe. This happens regardless of the presence of a leading edge suction peak at 4/5 of the sail height.

4.2 Dynamic variation of pressures and forces with a slightly overtrimmed spinnaker.

When sailing downwind, it is common practice to trim the spinnaker on the verge of luffing. In this section we discuss pressure and shape variation for a run in which the spinnaker was “overtrimmed”, i.e. the luff is not curling. During the period when the data were recorded, trimming, steering and crew positions were fixed.

The pressure and shape behaviour explained herein occurs several times throughout the test; the run

presented has been chosen as representative of all the runs.

In Figure 4 the ΔC_P variation for each of the pressure stripes along the sail for a 10 second run are shown. The horizontal axis is time while the vertical axes represent the percentage of sail curve and ΔC_P's are shown through the colourmap. Figure 5 shows CF_X, AWA and AWS variations for the same time period. Four times are highlighted in Figures 4 and 5 and they are named A, B, C and D. Sail shapes for frame A is shown in Figure 6. Shapes at the other frames are very similar, and differences are hardly noticeable, so they are not presented in the paper.

As shown in Figure 4, suctions are near maximum at frames A and C for all stripes. A leading edge suction peak is present at all stripes and CF_X is a maximum. Also the AWS has a local maximum, while AWA has little relationship with the driving force. At frames B and D CF_X, AWS and suctions for all stripes are minimum; ΔC_P distributions have similar trends to the ones at frames A and C, but the leading edge suction peaks disappear or become less pronounced.

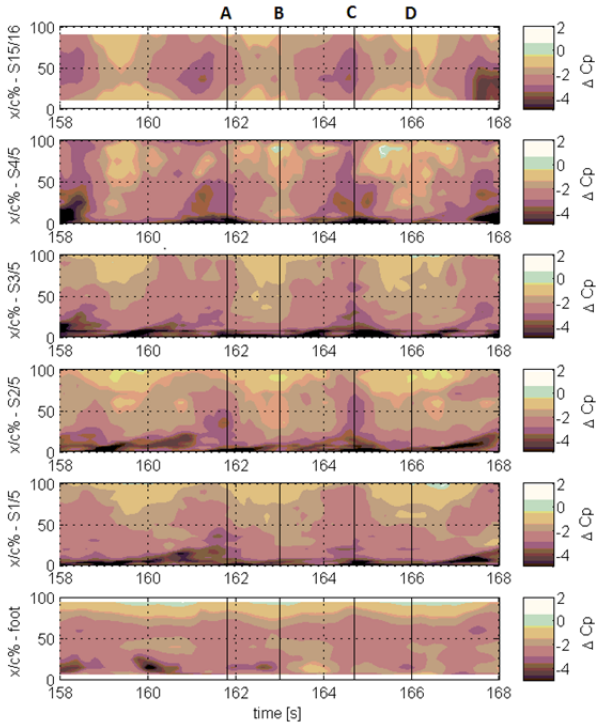

Figure 4: Space-time diagrams of ΔC_P: distribution along the curves (vertical axis), variation with time (horizontal axis) for all sections.

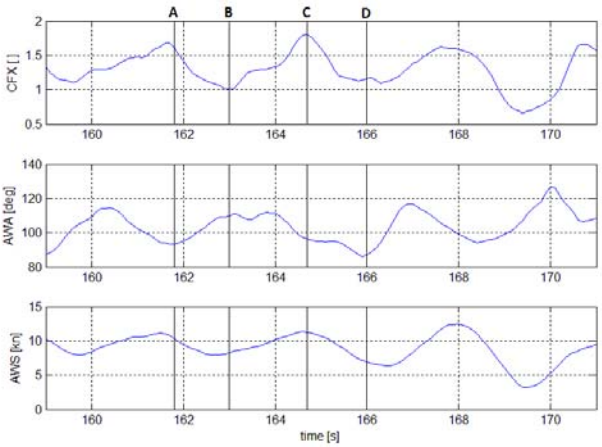

Figure 5: CF_X, AWA and AWS variation with time.

Figure 7 shows the ΔC_P distributions at stripe 2/5 as an example and highlights the change from low suction to high suction areas and vice-versa. A leading edge suction peak is often present, and it is more pronounced at frames A and C where suctions are highest. Note that in this situation (sail not luffing) suctions increase/decrease simultaneously along the chord (even if changes are biggest near the luff). This leads to big changes in CF_X, which varies as much as ±35% from its average value and, for instance, it increases of almost 80% of its initial value from B and C. The whole sail is "inflating" and "deflating" periodically, possibly driven by the changes in AWS and yacht motions, but the shape doesn't change significantly and is similar to that shown in Figure 6 throughout.

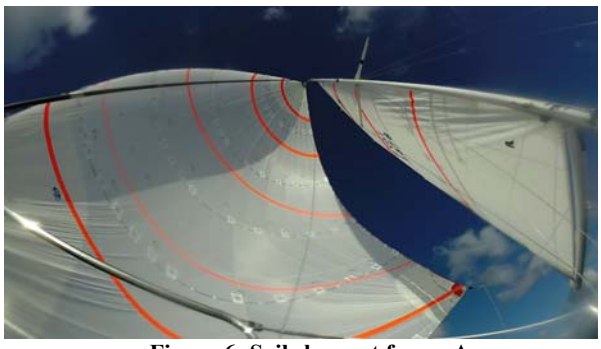

Figure 6: Sail shape at frame A.

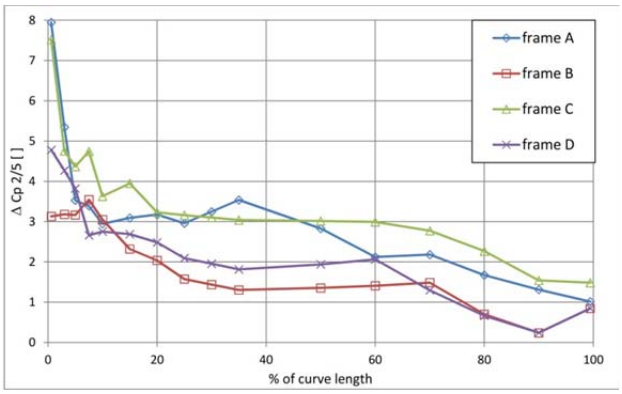

Figure 7: ΔC_P distributions at frames A, B, C and D for stripe 2/5.

4.3 Dynamic variation of pressures and forces with spinnaker luff curling

In this section we discuss pressure and shape variation for a run in which the spinnaker was slightly luffing while sailing, as is usual practice when sailing downwind. During the recorded time period, trimming, steering and crew position were fixed. The results shown herewith are extracted from a time period of about 20 seconds where the standard deviation of the AWA was below 5° and of AWS below 0.5 m/s. During this period the behaviour of the spinnaker was quite different from that analysed in section 4.2. The pressure and shape behaviour explained herewith occurs several times throughout the test; the run presented has been chosen as representative.

Similarly to section 4.2, Figures 8 and 9 show the ΔC_P, CF_X, AWA and AWS variation with time. Four instants are highlighted and named E, F, G and H in the figures. Figure 10 shows the sail shape at these four times.

Figure 10 shows that the spinnaker is not curling simultaneously throughout the whole luff, but curling occurs alternatively at two separate locations, one at the top part and one at the lower part of the luff respectively, which are named P1 and P2. Curling at P1 directly affects pressure at stripes S15/16, S4/5 and sometimes S3/5, while curling at P2 concerns pressure at S2/5 and S1/5.

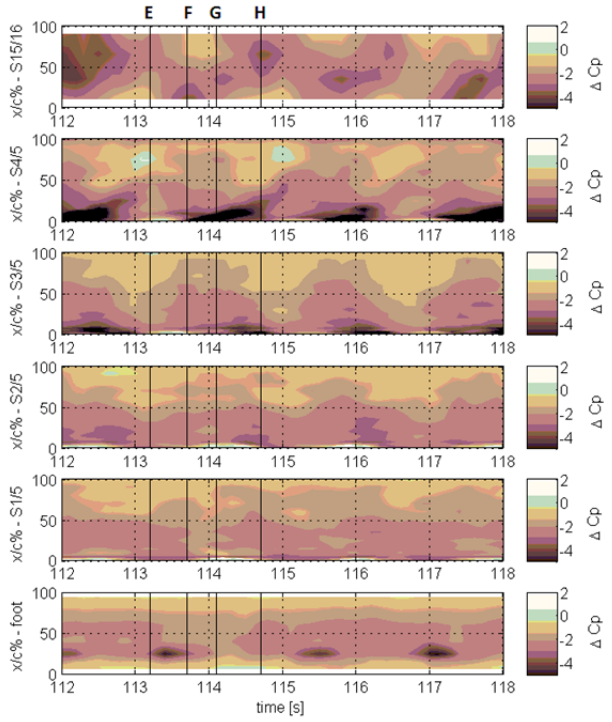

Figure 8: ΔC_P variation with time.

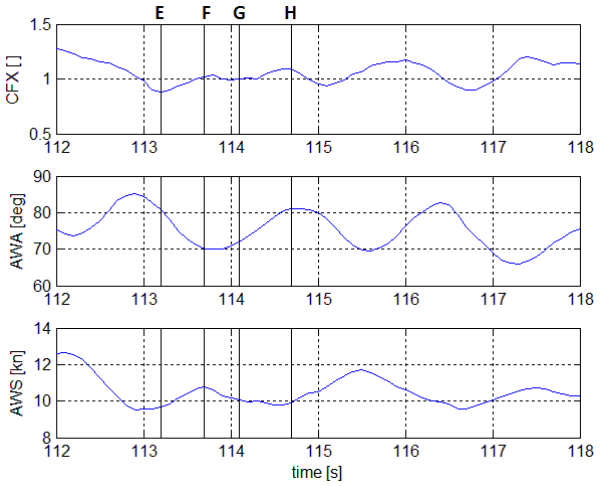

Figure 9: CF_X, AWA and AWS variation with time.

Consider a full sail shape (no curling) as the starting point for this investigation, as it is at t=113.0s (before frame E):

- At frame E, the luff is curling at P1. Suctions are low at S15/16, S4/5 and S3/5. CF_X is minimum at this stage, probably due to the highly reduced contribution of pressures at higher heights.
- From E to F, the curling "travels down" from P1 to P2. Suctions increase at stripes 15/16 and 4/5, while they decrease where curling occurs, at stripes 3/5 and 2/5. CF_X is recovering from its local minimum at this stage.
- At G the curling has "moved" to P2. Suctions are now lowest at S2/5, S1/5 and at the foot, while they have a maximum at S4/5 and S3/5. The overall aerodynamic force (which is not displayed on this paper) on the sail is still increasing compared to time F. In this particular case CF_X instead maintains a value similar to that in time F.
- From G to H, the shape recovers its full shape, and this can be considered as the completion of a cycle. Suctions recover at S1/5 and S2/5 near the luff, and all stripes settle at their new ΔC_P chord-wise distribution. Maxima of CF_X and CF_{TOT} occurs during the recovering of the sail shape. In this example, CF_X at time H is 21% higher than at time E.

During this period curling at parts P1 and P2 appear to alternate, as do the suctions. High suctions at part P1 correspond to low suctions at part P2 and vice-versa. The changes in sail shape and pressures appear to be related to AWA variations. AWA is maximised when the sail is full, it reduces when the sail starts folding at P1, it is minimised between frames F and G (during the curling) and it increases again when the sail shape recovers its shape. The AWS has little variation during this process.

When the top part of the sail is curling, a chord-wise "evolution" of suctions with time occurs at S4/5. ΔC_P distributions for stripe 4/5 at times E, F, G, H and at some intermediate instants are shown in Figure 11. These show that:

- At time E the luff is curling at S4/5 and the ΔC_P's are low, especially near the leading edge.
- At time F the suctions increase in the first 40% from the leading edge due to the top part of the sail filling up again after the curling. There is no leading edge suction peak yet.
- From time F to t=113.9s there is a big increase in suction in the first 5% of the chord.
- From t=113.9s to t=114.7s: the high suction region appears to travel towards the trailing edge. At the same time the region becomes broader in extent but gradually weaker in strength.
- At time H the cycle is almost completed. There is no leading edge suction peak, indicating that the top part of the sail is going to fold again.

A similar phenomenon occurs at section 15/16, with a suction increasing near the leading edge and travelling towards the trailing edge. In this case only 4 taps are available, so a less detailed analysis can be carried out. As shown in Figure 8, suctions increase at the leading edge (the first tap is placed at 10% of the chord) at time F. From times F to G the highest suction shifts towards the leech, reaching 25% of the curve by time G. However, in contrast to what happens at stripe 4/5, the suctions keep travelling on to reach 65% by time H. In other similar situations the high suctions seem to travel on across the whole section.

Therefore the resulting effect of the uncurling of the luff is a "suction shedding" or "evolution" towards the leech at stripes S4/5 and S15/16, which repeats quite consistently throughout the test. It can sometimes be seen at lower stripes, but it is at S4/5 and S15/16 that it occurs periodically throughout the whole test. The source of this suction development is unknown but it could be associated with the formation and shedding of a leading edge vortex [4]. Alternatively it may be created by the movement of the tip vortex shed behind the spinnaker head [4].

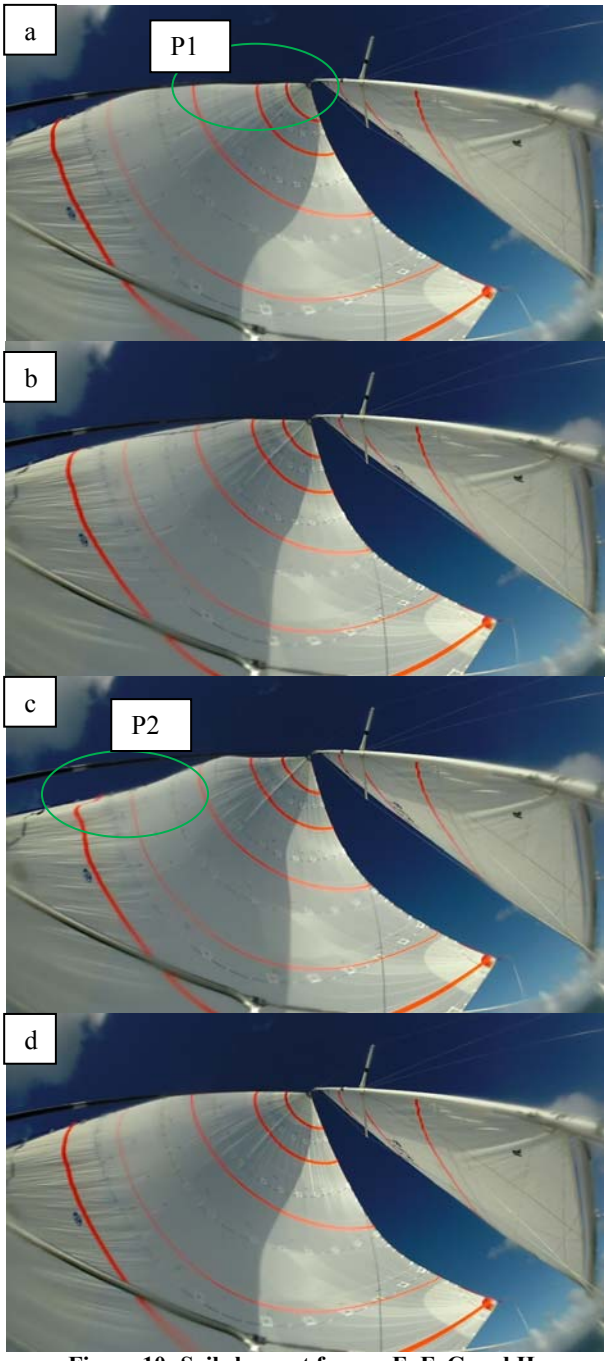

Figure 10: Sail shape at frames E, F, G and H.

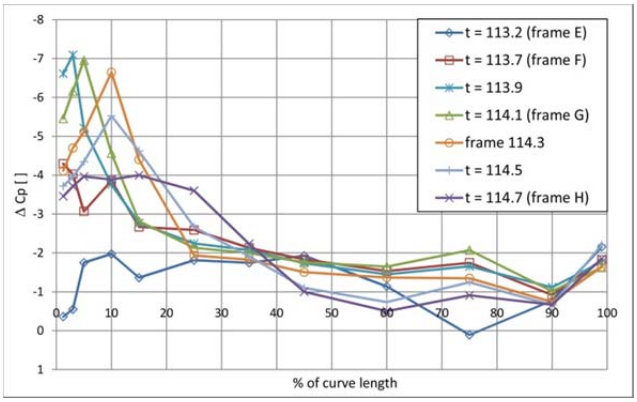

Figure 11: Chord-wise "suction evolution" at pressure stripe 4/5.

It is interesting to discuss the evolution of chord-wise pressures following to curling of the sail. A first example of this behaviour had been published in [14]. Figure 12 shows ΔC_P's for S3/5 at three different time instants across a curling and recovering of the shape, as it is been between instants E and H. The average ΔC_P distribution across the time period considered is shown with a dotted line as reference. Minimum suctions along the curve at a given stripe occur at the beginning of the curling. When the curling is at its maximum, suctions are lowest near the luff (the extent depending on how much the luff is folding), but bigger everywhere else. The recovery of the shape induces a sudden increase in suctions in the first 20% of the chord, and a pronounced leading edge suction peak. This is probably responsible for the increase in aerodynamic force as was discussed in regard to Figure 9. This phenomenon might be due to the quick deceleration of the luff when recovering its shape, which creates a "whiplash" giving a consequent added mass of air. It can also be related to a local increase of the flow speed amplifying locally the ΔC_P. Similar behaviour is found at lower stripes, but peaks in suctions are not so pronounced, as can be seen in figure 12.

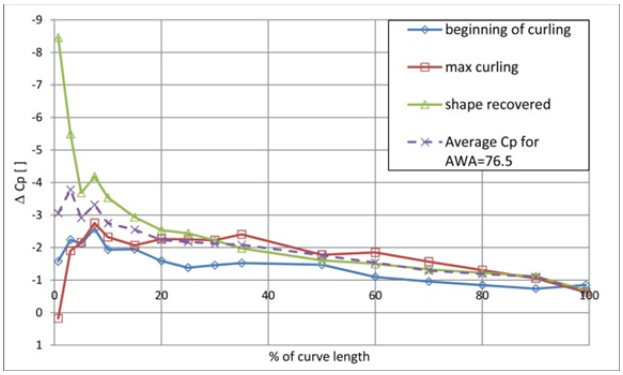

Figure 12: ΔC_P distributions at stripe 3/5 at start of curling, maximum curling, recovered shape and average ΔC_P

5. CONCLUSIONS

On water experiments have been carried out to investigate the dynamic behaviour of an asymmetric spinnaker in real sailing conditions. Yacht motions, wind characteristics, pressures and flying shape on an asymmetric spinnaker were simultaneously measured. Aerodynamic forces developed by the spinnaker were computed by the FEPV system.

Pressures were measured using 72 pressure sensors, distributed along six stripes at approximately $1/5^{th}$, $2/5^{th}$ $3/5^{th}$, $4/5^{th}$ of the sail height and, for the first time at full-scale, at the foot and close to the head ($15/16^{th}$ of the sail height).

Time averaged chord-wise pressure distributions at stripes S1/5 to S4/5 agree with previous full-scale publications [2, 8, 14]. Pressures along the foot were found to be non-zero at all AWAs, and mean differential pressure coefficients as high as -3.5 occurred at 25% of the chord. Suctions very close to the head were also non-zero, with the minimum mean ΔC_P being approximately -3.5 at 35% from the leading edge. Suctions close to the head have significant high values over the whole chord.

The dynamic behaviour of the asymmetric spinnaker has been analysed for two different spinnaker trims. In the first case the spinnaker was slightly overtrimmed, and sail was full at all times, while in the second situation the spinnaker was on the verge of luffing, as is common practice in downwind sailing.

When the spinnaker is slightly overtrimmed, suctions increase/decrease simultaneously along the chord and at all heights. This affects the entity of CF_X, which varies as much as ±35% from its average value despite little variation of AWA. Chord-wise ΔC_P distributions present a leading edge suction peak at all time, which is more pronounced when the suctions are highest over the chord.

When the trim is optimal, the sail is luffing almost periodically. The curling alternates at two separate locations, at the top and at the lower part of the luff respectively, as do the suctions. When the sail is luffing at the top part, the suctions are highest in the bottom (full) part and vice-versa. The CF_X variations are driven by the different contributions from the pressures at the top and bottom part of the spinnaker. Generally CF_X is a minimum when the top part of the sail is curling and a maximum after the bottom part is curling, when the sail is recovering its full shape.

The uncurling of the luff leads to the development of a leading edge suction peak in the first 5% from the luff for stripe S4/5, and then to a "suction shedding" towards the leech up to 25% of the curve length. Similar pattern is found at S15/16, but suctions keep traveling on to reach 65% of the curve and, sometimes, across the whole section.This phenomenon could be associated with the formation and shedding of a leading edge vortex. Alternatively it may be created by the movement of the tip vortex shed behind the spinnaker head.

At stripes 3/5 and 4/5, the recovery of the shape after a curling induces a sudden increase in suction in the first 20% of the chord, and a pronounced transient leading edge suction peak. This phenomenon might be due to the quick deceleration of the luff when recovering its shape, which creates a "whiplash" giving a consequent added mass of air. It can also be related to a local increase of the flow speed amplifying locally the ΔC_P.

Findings from this work show that full-scale measurement of pressure and shape in dynamic conditions is a feasible task, and important insight into the aerodynamics of sails can be made.

References

1. Le Pelley, D., Richards, P., (2011), "Effective Wind Tunnel Tesing of Yacht Sails Using a Real-Time Velocity Prediction Program",*20th Cheasapeake Sailing Yacht Symposium, March 18th-19th, Annapolis, Maryland, USA.*
2. Viola, I.M., Flay, R.G.J., (2009),"Force and pressure investigation of modern asymmetric spinnakers", *Internation Journal of Small Craft Technology, Transaction RINA, 151(2):31-40.*
3. Richards, P.J., Lasher, W., (2008), "Wind Tunnel and CFD Modelling of Pressures on Downwind Sails", *BBAA VI International Colloquium on Bluff Bodies Aerodynamics & Applications, July 20th-24th, Milano, Italy*.
4. Viola, I.M., Bartesaghi, S., Van-Renterghem, T., Ponzini, R.,(2014), "Detached Eddy Simulation of a sailing yacht", *Ocean Engineering, 90: 93-103.*
5. Durand, M., Lothode, C., Hauville, F., Leroyer, A., Visonneau, M., Floch, R., (2013), "FSI Investigation on Stability of Downwind Sails with an Automatic Dynamic Trimming", in *3rd International Conference On Innovation in High Performance Sailing Yachts, June 26th-29th, Lorient.*
6. Wright, A.M., Claughton, A.R., Paton, J., Lewis, R., (2010). "Off-Wind Sail Performance Prediction and Optimisation", *The Second International Conference on Innovation in High Performance Sailing Yachts, June 30th- July 1st, Lorient, France.*
7. Le Pelley, D.J., Morris, D., Richards, P.J., (2012). "Aerodynamic force deduction on yacht sails using pressure and shape measurement in real time", *4th High Performance Yacht Design Conference, March 12th-14th, Auckland, New Zealand.*
8. Motta, D., Flay, R.G.J., Richards, P.J., Le Pelley, D.J., Deparday, J., Bot, P., (2014), "Experimental Investigation of Asymmetric Spinnaker Aerodynamics Using Pressure and Sail Shape Measurements", *Ocean Engineering, 90: 104-118.*
9. Graves, W., T. Barbera, J.B. Braun, L. Imas, (2008) "Measurement and Simulation of Pressure Distribution on Full Size Sails", *3rd High Performance Yacht Design Conference, December 1st-4th, Auckland.*
10. Augier, B., Bot, P., Hauville, F., Durand, M., (2012), "Experimental validation of unsteady models for fluid structure interaction: Application to yacht sails and rigs". *Journal of Wind Engineering and Industrial Aerodynamics 101(0): 53-66.*
11. Bergsma, F., Motta, D., Le Pelley, D.J., Richards, P.J., Flay, R.G.J., (2012). "Investigation of shroud tension on sailing yacht aerodynamics using full-scale real-time pressure and sail shape measurements", *22nd International HISWA Symposium on Yacht Design and Yacht Construction, November 12th-13th, Amsterdam*.
12. Hochkirch, K., (2000). "Design and Construction of a Full-Scale Measurement System for the Analysis of Sailing Performance", *Technical University of Berlin, PhD Thesis.*
13. Masuyama, Y., Fukasawa,T., (2009). "Database of sail shapes versus sail performance and validation of numerical calculations for the upwind condition", *Journal of Marine technologies, Vol.14(2), pp.137-160.*
14. Deparday, J., Bot, P., Hauville, F., Motta, D.,Le Pelley, D.J., Flay, R.G.J., (2014), "Dynamic measurements of pressures, sail shape and forces on a full-scale spinnaker", 23rd *International HISWA Symposium on Yacht Design and Yacht Construction, November 17th-18th, Amsterdam.*
15. Le Pelley, D.J., Modral, O., (2008), "VSPARS: A combined sail and rig shape recognition system using imaging techniques", *3rd High Performance Yacht Design Conference, March 12th-14th, Auckland, New Zealand.*
16. Flay, R.G.J., Millar, S., (2006), "Experimental Considerations Concerning Pressure Measurements on Sails: Wind Tunnel and Full-Scale", *2nd High Performance Yacht Design Conference, December 1st-4th, Auckland, New Zealand.*